

Numerical simulation of the plasma–MIG process—interactions of the arcs, droplet detachment and weld pool formation

M. Hertel · U. Füssel · M. Schnick

Received: 17 October 2012 / Accepted: 16 August 2013 / Published online: 31 August 2013
© International Institute of Welding 2013

Abstract The plasma–metal inert gas (MIG) process is characterized by a variety of process parameters. Numerical simulation can be used to investigate the influence of these process parameters and thus helps to improve the properties of the weld. In this paper we discuss a procedure to describe the plasma–MIG process by coupling numerical models of the arc and the droplet detachment with a three-dimensional model for the plasma–MIG weld pool. Using the magnetohydrodynamic (MHD) arc model, the effects of process parameters on the arc pressure profile and the energy input profile on the workpiece can be analyzed. The volume-of-fluid (VoF)–MHD model of the droplet detachment describes the properties of the resulting droplet in terms of its size, temperature and speed. In the three-dimensional VoF model of the weld pool, the influences of the arc and the droplet are simplified by source terms in the mass, momentum and energy equations. Due to these simplifications in the physical complexity, the process and the seam shape can be described with reasonable computational effort.

Keywords Simulating · Plasma–MIG welding · GMA welding · Liquids · Arc welding · Particles · Molten pool

1 Introduction

The plasma–metal inert gas (MIG) process is a combination of a MIG and a plasma arc process. In the hybrid process, both arcs are established between a welding torch and a common weld pool at a workpiece. Two different configurations are

known, the inline configuration with a leading plasma tungsten arc and a trailing MIG arc and the concentric configuration with a central MIG process surrounded by a plasma arc. The second configuration offers many advantages concerning the welding speed, the process reliability and the ability to determine the size of the weld pool and penetration [1]. However, the process is also quite complex, since a huge number of process parameters and design features influence the weld properties.

In order to get a better understanding of the cause and effect, chains and their sensitivity numerical simulation become more and more important. Besides visualization and characterization, the modelling is aimed to enable predictions of the process stability as well as reliable predictions of the properties of the weld and the heat distribution in the workpiece as a function of the parameters of the process. Due to the model complexity and the associated computational effort, there is still no uniform model of the plasma–MIG or at least the MIG process in which the properties of the weld seam could be calculated physically self-consistently as a function of the process parameters. Instead, it is common practice in modelling to focus on a part of the process, such as the weld pool, the droplet transfer or the arc. Many models of the gas metal arc welding (GMAW) weld pool do not include the wire, the plasma and the droplet transfer in the weld pool. Instead, these influences are approximated by source terms (e.g. [2, 3]). Models of the droplet transfer include the wire and the arc plasma, but either uses a two-dimensional axisymmetric geometry and is therefore not suitable to calculate the seam shape (e.g. [4]) or uses a three-dimensional geometry but neglects the energy flow in the wire [5]. In arc models of the GMAW process, the arc properties at the surface of the workpiece could be described as a function of the process parameters, but in the models, the electrodes are assumed to be not molten and therefore considered as solids with a given shape constant in time (e.g. [6]) or as a function of time (e.g. [7]). In

Doc. IIW-2411, recommended for publication by Study Group SG-212 “The Physics of Welding”.

M. Hertel (✉) · U. Füssel · M. Schnick
Technische Universität Dresden, Dresden, Germany
e-mail: martin.hertel@tu-dresden.de

all these models, insufficient simplifications or assumptions which must be verified by experiments have been used.

In this work we present a procedure based on the simulation software ANSYS CFX, in which the benefits of the individual models are combined. With the combined model, the properties of the joint could be calculated with respect to the process parameters but without having to use experimental investigations in a wide range of parameters (Fig. 1). With the arc model, we calculate the arc pressure and the heat flux profile at the surface of the workpiece. The shape, velocity and temperature of the detached droplet are calculated with the droplet transfer model. The data of the arc and the droplet transfer model is then used in the weld pool model. In the following chapters, these models will be discussed more in detail.

2 Arc model

The plasma–MIG arc model is used to investigate the physical processes in the arc. Of particular interest are the properties of the arc at the workpiece, especially in dependence of process

parameters. The droplet transfer is neglected and the workpiece is assumed to be flat. In the model, the electrodes and the components of the welding torch are considered as solids. To take into account the influence of welding speed, we use a mirror-symmetric geometry (Fig. 2a).

The following MHD equation system is used to calculate the properties of the arc:

$$\frac{\partial \rho}{\partial t} + \nabla \cdot (\rho \vec{u}) = 0 \quad (2.1)$$

$$\frac{\partial (\rho \vec{u})}{\partial t} + \nabla \cdot (\rho \vec{u} \otimes \vec{u}) = -\nabla p + \nabla \cdot \tau + \vec{j} \times \vec{B} \quad (2.2)$$

$$\frac{\partial (\rho h_g)}{\partial t} + \nabla \cdot (\rho \vec{u} h_g) = \frac{\partial p}{\partial t} + \nabla \cdot (\lambda \nabla T_g) + \frac{j^2}{\sigma} + Q_{RAD} \quad (2.3)$$

$$\frac{\partial (\rho h_m)}{\partial t} + \nabla \cdot (\rho \vec{u}_{weld} h_m) = \nabla \cdot (\lambda \nabla T_m) + \frac{j^2}{\sigma} \quad (2.4)$$

Fig. 1 Calculation of the joint properties in dependence of the plasma–MIG process parameter due to the coupling of an arc model and a droplet transfer model with a weld pool model

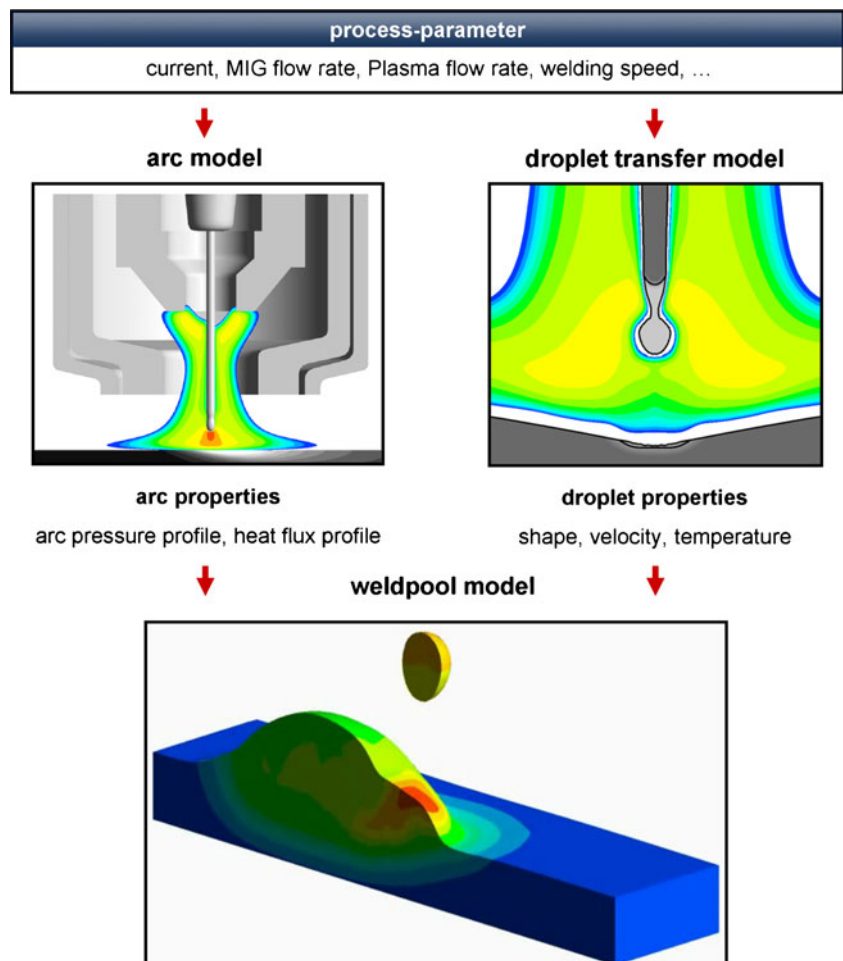
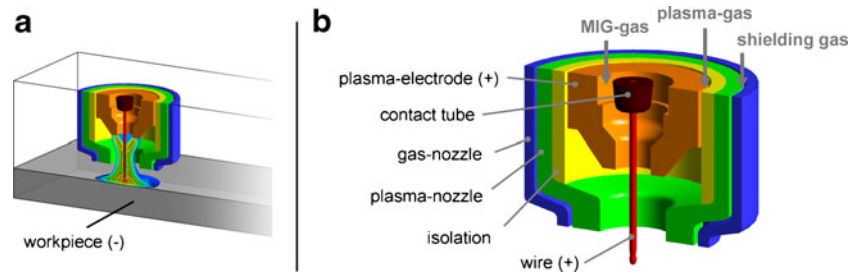


Fig. 2 Computational domain of the mirror-symmetric arc model (a) and components of the plasma welding torch from Alaluss et al. [1] (b)



$$\nabla \cdot (\sigma \nabla \phi) = 0 \tag{2.5}$$

$$\Delta \vec{A} = -\mu_0 \cdot \vec{j} \tag{2.6}$$

In Eqs. 2.1–2.6, ρ is the density, t is the time, u is the velocity vector, p is the pressure, τ is the stress tensor, j is the electrical current density, B is the magnetic field, h_g is the enthalpy of the shielding gas, λ is the thermal conductivity, T_g is the temperature of the shielding gas, σ is the electrical conductivity, Q_{RAD} is the net emission coefficient, h_m is the enthalpy of the workpiece (metal), T_m is the temperature of the workpiece, φ is the electric potential, A is the magnetic vector potential and μ_0 is the magnetic permeability.

To save costs, we resign the calculation of temperature distribution within the plasma torch and the interactions in the sheath regions. Instead, we define a heat loss term on the gas side of the gas–solid interfaces of the wire and plasma electrodes to estimate the convective heat transfer of heavy particles from plasma to solid surfaces (Eq. 2.7). The formulation is based on an integral conductivity [7] and an assumed length for the anodic sheath region of 0.1 mm [8]. To consider the effect of welding speed on the arc properties, we use a simplified formulation for the energy balance in the workpiece, which includes the advection term (second term on the left-hand side of Eq. 2.4). At the solid side of the gas–solid interface, we include a heat flux to display the effect of the non-thermionic sheath region, according to the formulation of Lowke and Tanaka [9].

$$\hat{q}_{gas\ side} = \int_{T_{solid}}^{T_{gas}} \lambda(T) dT / 0.1\ mm \tag{2.7}$$

$$\hat{q}_{workpiece} = \left| \vec{j} \times \vec{n} \right| \cdot (15.8\ V - 4.5\ V) \tag{2.8}$$

The material properties and net emission coefficient of argon from Murphy [10] and Menart and Malik [11] are used for the shielding gas. The influence of metal vapour is neglected in this study. The components of the welding torch

are made of copper. For the wire electrode and the workpiece, we use the material properties of stellite 6 [1].

By sensitivity studies, the influence of process parameters on the arc properties was examined. Main influential variables are the MIG, plasma and shielding gas flow rates (V indicates the volume flow rate) (Fig. 2b) and the current of the MIG and plasma process. The flow rates have only a minor influence on the arc properties at the workpiece (Fig. 4, left) but a high influence on the stability of the process.

At MIG flow rates of 5 l/min and a plasma current of 140 A, the model predicts a spot attachment of the arc at the plasma electrode (Fig. 3b). At MIG flow rates over 5 l/min, the gas flow is not ionized uniformly over the circumference and the process gets unstable. This fact is consistent with experiences from experimental studies [1].

In contrast to the flow rate, the MIG and plasma current have a large influence on the arc pressure and the heat flux profile at the surface of the workpiece (Fig. 4). The arc pressure is shown as a relative pressure related to the atmospheric pressure. The heat flux profile at the workpiece includes both the convective heat transfer from the arc and the sheath heating at the cathodic workpiece.

A rise in the MIG current leads mainly to an increase of the profiles. The increase of the plasma current results in a broadening of the profiles. In a good approximation, the profiles could be considered as rotationally symmetrical.

3 Droplet transfer model

The droplet transfer model is used to investigate the physical processes during the detachment of the droplet taking into account the influence of the arc. The model is based on the volume-of-fluid method, described by Hirt and Nichols [12]. The electrodes and the gas are considered as an immiscible two-phase mixture, which are separated from each other by a phase boundary (the surface of the electrodes). The components of the welding torch are considered as solids (Fig. 5). To reduce computational time, we assume rotational symmetry.

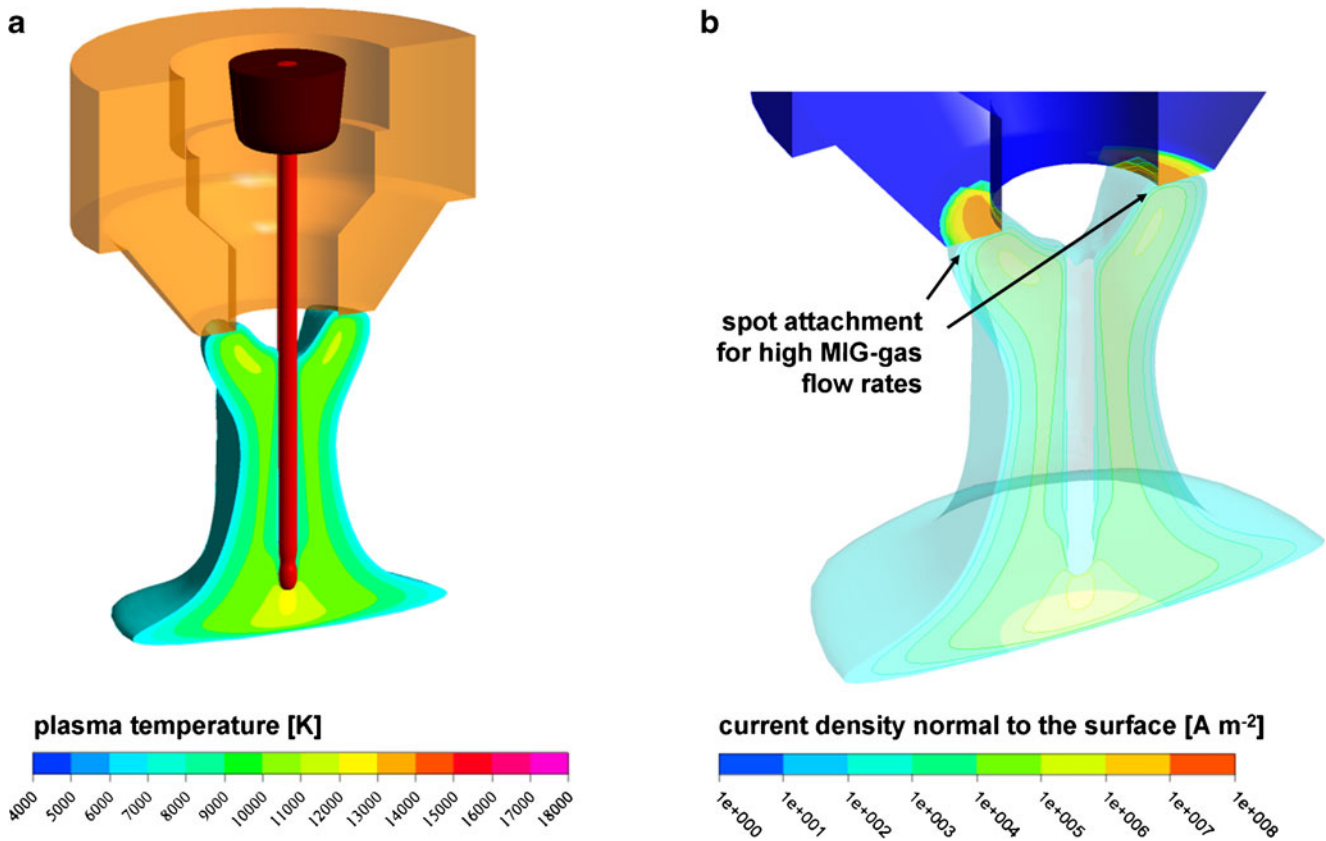


Fig. 3 Calculated arc temperature distribution (a) and current density distribution at the plasma electrode (b). Process parameters: $I_{MIG}=169$ A, $I_{Plasma}=140$ A, $V_{MIG}=5$ l/min, $V_{Plasma}=10$ l/min, $V_{Shielding}=18$ l/min

Fundamental is the transport equation for the volume fraction F_m of the liquid phase and the volume fraction F_g of the gaseous phase.

$$\frac{\partial F_m}{\partial t} + \nabla \cdot (F_m \vec{u}) = 0, \quad F_g = 1 - F_m \quad (3.1)$$

The density, viscosity and electrical conductivity of the multiphase mixture are calculated as a function of the volume fractions of the phases.

$$\rho = F_g \rho_g + F_m \rho_m \quad (3.2)$$

$$\eta = F_g \eta_g + F_m \eta_m \quad (3.3)$$

$$\sigma = F_g \sigma_g + F_m \sigma_m \quad (3.4)$$

Assuming a uniform flow field for both phases, the conservation equations for mass and momentum correspond to those for the single-phase formulation (Eqs. 2.1 and 2.2). Two additional source terms are added to the right-hand side of the momentum equation. F_{ST} is the vector of the surface tension force according to the continuum surface force model of Brackbill et al. [13], and F_{SLD} is a source term to display the behaviour of the

solid regions in the liquid phase regarding its velocities. The Maxwell equations for the electrical current and the magnetic vector potential (Eqs. 2.5 and 2.6) remain unchanged.

$$\vec{F}_{ST} = -\gamma_{gm} \nabla \cdot \left(\frac{\nabla F_m}{|\nabla F_m|} \right) \frac{\nabla F_m}{|\nabla F_m|} \quad (3.5)$$

$$\vec{F}_{SLD} = -10^{10} \frac{N}{m} \frac{m^{-3}}{s^{-1}} (\vec{u} - \vec{u}_{solid}) \quad (3.6)$$

For both phases, separate energy conservation equations are calculated.

$$\frac{\partial (F_g \rho h_g)}{\partial t} + \nabla \cdot (F_g \rho \vec{u} h_g) = \nabla \cdot (\lambda_g \nabla T_g) + F_g \frac{j^2}{\sigma} + F_g Q_{RAD} - Q_{HT} \quad (3.7)$$

$$\frac{\partial (F_m \rho h_m)}{\partial t} + \nabla \cdot (F_m \rho \vec{u} h_m) = \nabla \cdot (\lambda_m \nabla T_m) + F_m \frac{j^2}{\sigma} + F_m Q_{SRF} + Q_{HT} \quad (3.8)$$

The source term Q_{HT} represents the energy exchange between the phases, and Q_{SRF} displays the heat flow at

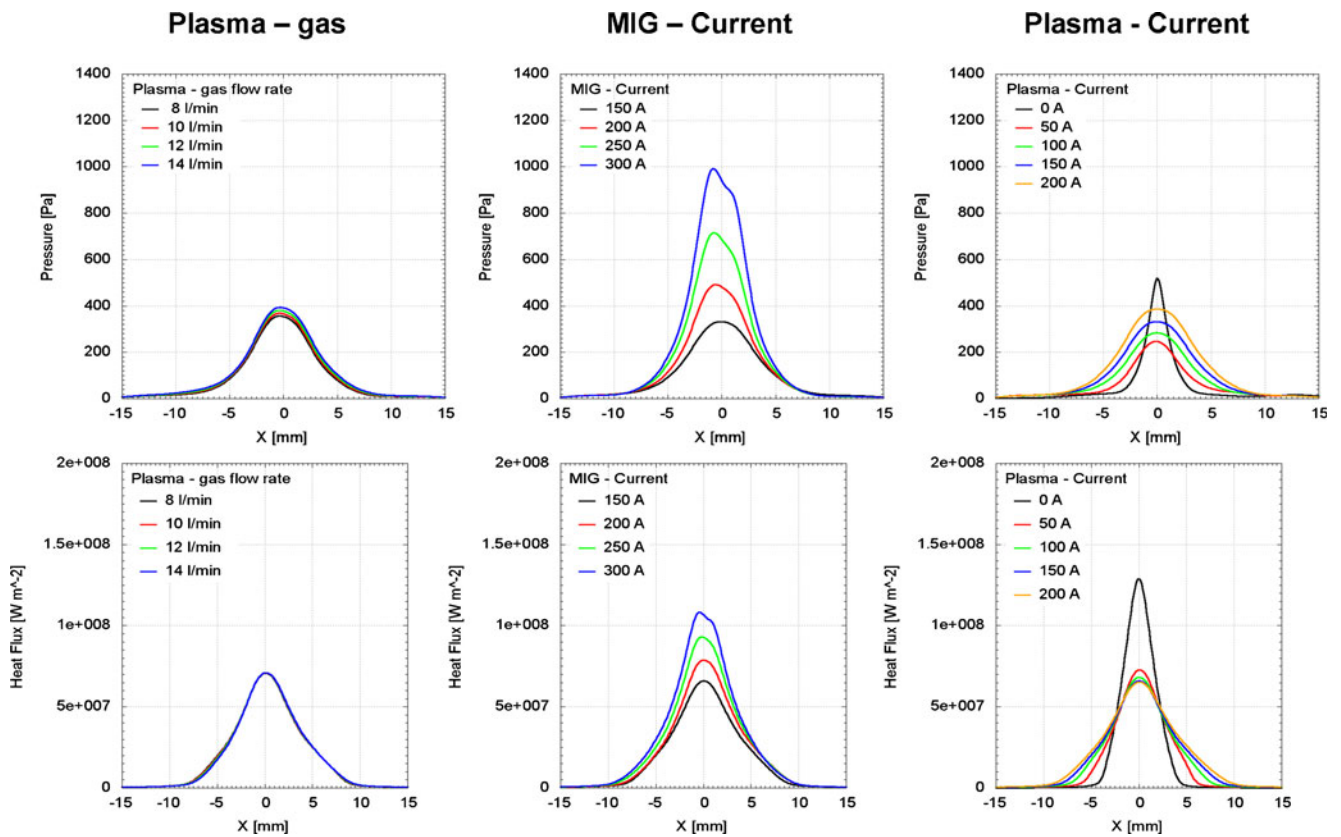


Fig. 4 Sensitivity studies regarding the influences of the process parameters: plasma gas (*left*), MIG current (*middle*) and plasma current (*right*), on the arc pressure profile (relative pressure) (*top*) and the heat flux

profile (*bottom*) at the surface of the workpiece. Reference process parameters: $I_{MIG}=150$ A, $I_{Plasma}=150$ A, $V_{MIG}=4$ l/min, $V_{Plasma}=10$ l/min, $V_{Shielding}=18$ l/min

the phase boundary (metal surface), including sheath heating, vaporization cooling and radiation. In the anodic sheath region, we assume that the electric current is carried by electrons only. Therefore, the energy input in the sheath region equals the product of the current density

normal to the surface $\left| \vec{j} \cdot \nabla F_m \right|$ and the recombination energy of electrons of $\phi_{SH}=4.5$ V.

$$Q_{HT} = \int_{T_m}^{T_g} \lambda(T) dT / 0.1 \text{ mm} \cdot \nabla F_m \tag{3.9}$$

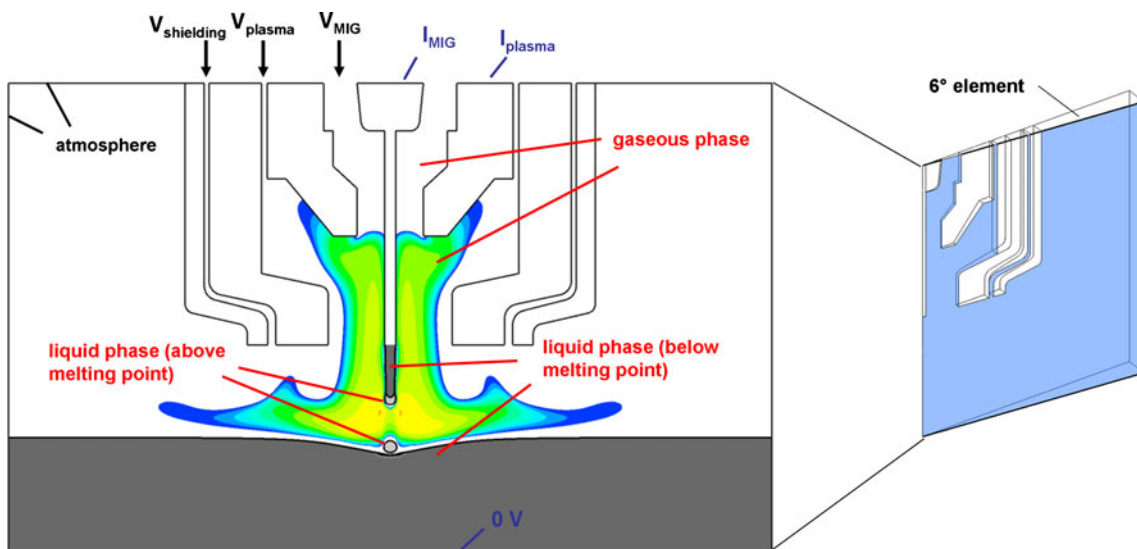


Fig. 5 Computational domain and boundary conditions of the axisymmetric droplet transfer model

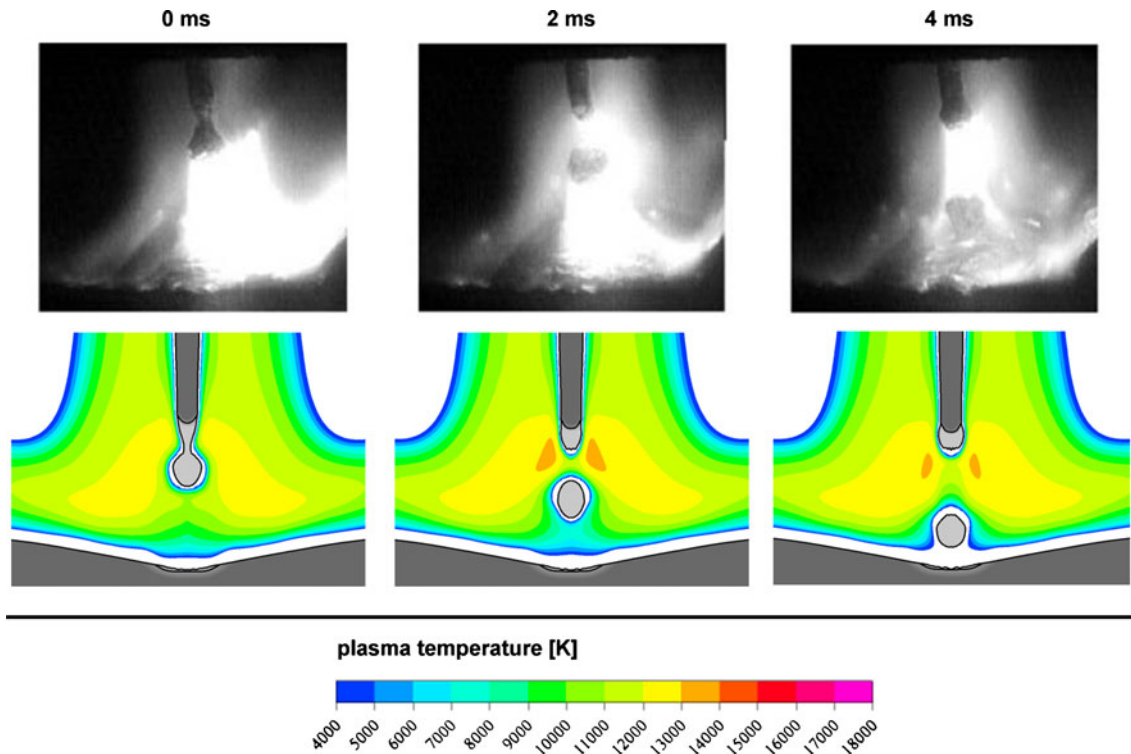


Fig. 6 Comparison of the calculated droplet shapes with the experiment from Alaluss et al. [1]. Process parameters: $I_{MIG}=273$ A, $I_{Plasma}=140$ A, $V_{MIG}=5$ l/min, $V_{Plasma}=10$ l/min, $V_{Shielding}=18$ l/min

$$Q_{SRF} = \underbrace{|\vec{j} \cdot \nabla F_m| \cdot \varphi_{SH}}_{\text{Sheath heating}} - \left[\underbrace{\dot{m}_{VAP} h_{VAP}}_{\text{Vaporization}} + \underbrace{0.5 \sigma_{SB} (T_m^4 - (300 \text{ K})^4)}_{\text{Radiation}} \right] \cdot |\nabla F_m| \tag{3.10}$$

In our calculation, we use the material properties of pure argon for the gaseous phase and the properties of stellite 6 for the liquid phase.

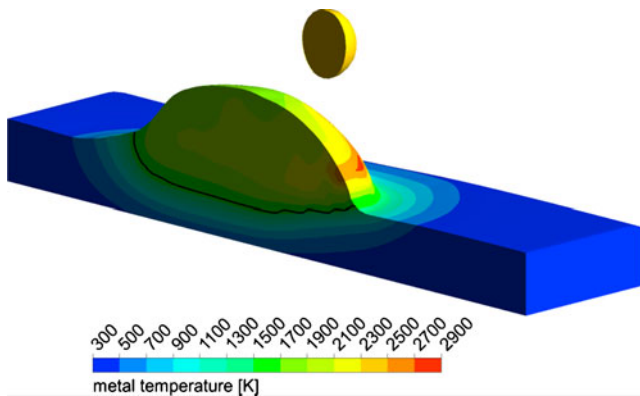


Fig. 7 Calculated temperature distribution (colour scale) and melting line (black line) in the weld seam. Process parameters: $I_{MIG}=169$ A, $I_{Plasma}=140$ A, $V_{MIG}=5$ l/min, $V_{Plasma}=10$ l/min, $V_{Shielding}=18$ l/min

The presented model combines for the first time an arc model with a droplet transfer model for the plasma–MIG process. Figure 6 shows exemplarily the temperature distribution in the arc and a comparison of the calculated droplet shapes with the experiment for a MIG current of 273 A and a plasma current of 140 A.

A major influence on the droplet detachment during plasma–MIG welding results from the current path at the wire electrode. For the plasma–MIG process, the current densities at the wire are lower in comparison to those for a MIG process. The reason is the surrounding gas, which is already ionized. This determines not only the distribution of the electromagnetic pinch force but also the distribution of the current density and, as a result, the sheath heating. It is expected that this will result in lower fume emissions at the wire.

The largest part of the energy input into the wire electrode results from the recombination of electrons in the anodic sheath region (1,200 W), the pre-heating effect due to resistive heating of the wire (450 W) and the convective heat transfer from the arc (300 W). The cooling heat flow due to vaporization (–50 W) and surface radiation (–20 W) is much smaller.

4 Weld pool model

The weld pool model is used to investigate the physical processes during the formation of the weld seam. Based on the calculated variables such as the temperature distribution in the workpiece, conclusion about the shape and the properties of the weld could be made. For the representation of the process, at least a mirror-symmetrical model with a sufficiently large length in the direction of welding is required. This leads to a high number of mesh elements and thus to a high computational effort. To limit the computational time, it is common to reduce the complexity of the equation system. For this purpose, the influences of the arc and the droplet transfer model are approximated by source terms in the mass, momentum and energy equations [1–3]. These source terms are often determined empirically and described only a limited dependence of the process parameters.

In the presented procedure, we use the results of the arc and the droplet transfer model to describe the variations of the source terms with the process parameters without having to perform experimental investigations in a wide parameter

range. The arc can be reduced to its force (arc pressure) and its heat input on the surface of the weld pool. The calculated variation of the arc pressure and the heat input in dependence of the process parameters is shown in Fig. 4. The droplet transfer could be approximated due to a mass source term, M_{DR} , which is defined as a function of the transfer rate and includes the shape, velocity and temperature of the droplet in the model. Based on the volume-of-fluid approach, the conservation equations for mass, momentum and energy read as follows:

$$\text{Mass} \quad \frac{\partial \rho}{\partial t} + \nabla \cdot (\rho \vec{u}) = \underbrace{M_{DR}}_{\text{Droplet Mass Source}} \quad (4.1)$$

$$\text{Momentum} \quad \frac{\partial (\rho \vec{u})}{\partial t} + \nabla \cdot (\rho \vec{u} \otimes \vec{u}) = \nabla \cdot \tau + \underbrace{\rho \vec{g} \beta_T (T_m - T_0)}_{\text{Buoyancy}} + \underbrace{\vec{F}_{ST}}_{\text{Surface Tension}} + \underbrace{\vec{F}_{SLD}}_{\text{Solid Force}} + \underbrace{p_{ARC}(\vec{x}) \cdot \nabla F_m}_{\text{Arc Pressure}} + \underbrace{M_{DR} \vec{u}_{DR}}_{\text{Droplet Velocity}} \quad (4.2)$$

$$\text{Energy} \quad \frac{\partial (\rho h_m)}{\partial t} + \nabla \cdot (\rho \vec{u}_{weld} h_m) = \nabla \cdot (\lambda \nabla T_m) + \left[\underbrace{\dot{q}_{ARC}(\vec{x})}_{\text{Arc Heat Input}} - \underbrace{\dot{m}_{VAP} h_{VAP}}_{\text{Vaporization}} - \underbrace{0.5 \sigma_{SB} (T_m^4 - (300 \text{ K})^4)}_{\text{Radiation}} \right] \cdot |\nabla F_m| + \underbrace{M_{DR} h_{DR}}_{\text{Droplet Enthalpy}} \quad (4.3)$$

Figure 7 shows the calculated shape and temperature distribution for a plasma–MIG weld pool with the given process parameters. The point of highest temperature is assigned to the maximum of the energy flux of the arc. The entering of the droplet leads to a strong mixing of the weld pool material. Therefore, the mean temperatures are lower in the weld pool. The cooling effect due to the heat flow in the workpiece itself is much greater than the cooling effect due to the heat radiation and vaporization at the surface of the weld pool.

The most important advantage of this procedure is that there are no experimental studies necessary to reflect the influence of process parameters in the weld pool model.

5 Conclusions

In this paper we discussed a numerical procedure to describe the properties of the plasma–MIG joint as a function of the process parameters. Due to the combination of an arc and a

droplet transfer model with a model of the weld pool, we could combine the advantage of the models and reduce the computational effort.

The calculations predict a high influence of the MIG flow rate on the process stability. At MIG flow rates over 5 l/min, the gas flow is not ionized uniformly over the circumference and the process gets unstable. This fact is consistent with experiences from experimental studies. The arc pressure and the heat flux profile at the surface of the workpiece are mainly influenced by the MIG and plasma current. Due to the surrounding plasma arc, the arc attachment at the wire is less concentrated and the current densities are lower. Therefore, the arc pressure of the plasma–MIG process in comparison to that of a MIG process is lower, and the profiles for the arc pressure and heat flux are broader.

The implementation of the pressure and heat flux profiles from the arc model and the droplet properties from the droplet transfer model as a function of the process parameters allows the calculation of the joint properties without having to use experimental investigations.

References

1. Alaluss K, Bürner G, Gehde M (2010) Simulation of weld pool in plasma–MIG deposition welding. In: 9th international seminar on numerical analysis of weldability, Graz, 28–30 Sept 2009.
2. Kumar A, DebRoy T (2007) Heat transfer and fluid flow during gas-metal-arc welding for various joint configurations and welding positions. *Metall Mater Trans A* 38:506–519
3. Guo H, Hu J, Tsai HL (2010) Three-dimensional modeling of gas metal arc welding of aluminum alloys. *J Manuf Sci Eng* 132(2):021011
4. Haidar J, Lowke JJ (1996) Predictions of metal droplet formation in arc welding. *J Phys D Appl Phys* 29(12):2951
5. Xu G, Hu J, Tsai HL (2008) Three-dimensional modeling of the plasma arc in arc welding. *J Appl Phys* 104(10):103301
6. Schnick M, Füssel U, Hertel M, Spille-Kohoff A, Murphy AB (2010) Metal vapor causes a central minimum in arc temperature in gas–metal arc welding through increased radiative emission. *J Phys D Appl Phys* 43:022001
7. Lowke JJ (1997) A unified theory of arcs and their electrodes. *J Phys IV France* 07:C4-283–C4-294
8. Finkelnburg W, Segal SM (1951) The potential field in and around a gas discharge, and its influence on the discharge mechanism. *Phys Rev* 83:582–585
9. Lowke JJ, Tanaka M (2008) The physics of non-thermionic cathodes of electric arcs. In: Gas discharges and their applications. 17th international conference on gas discharges and their applications, 2008 (GD 2008), Cardiff, 7–12 Sept, pp. 137–140
10. Murphy AB (2001) Thermal plasmas in gas mixtures (Topical Review). *J Phys D Appl Phys* 34:151–173
11. Menart J, Malik S (2002) Net emission coefficients for argon–iron thermal plasmas. *J Phys D Appl Phys* 35:867–874
12. Hirt CW, Nichols BD (1981) Volume of fluid (VOF) method for the dynamics of free boundaries. *J Comput Phys* 39:201–225
13. Brackbill JU, Kothe DB, Zemach C (1992) A continuum method for modeling surface tension. *J Comput Phys* 100:335–354